Water Air Soil Pollut (2024) 235:63
https://doi.org/10.1007/s11270-023-06875-8

Green Synthesis of Date Palm Seed Extract–Derived Iron Sulfide Nanoparticles for Effective Removal of Hexavalent Chromium

Fatemah Habib · Abdallah Shanableh · Sourjya Bhattacharjee · Mohamed Abdallah

Received: 1 July 2023 / Accepted: 26 December 2023 / Published online: 6 January 2024
© The Author(s), under exclusive licence to Springer Nature Switzerland AG 2024

Abstract In this study, we investigated the removal of hexavalent chromium (Cr(VI)) through an innovative approach, which employed iron sulfide nanoparticles synthesized via a green chemistry technique, utilizing extracts derived from date palm seeds (referred to as ds-FeS). Batch studies, which were well represented by the Langmuir isotherm model, were conducted to determine the maximum removal capacities (q_m) of ds-FeS nanoparticles at three different initial pH conditions (pH = 3, 7, and 9). Additionally, batch kinetic studies were conducted under varying conditions of initial Cr(VI) load (3.5, 9, 27, and 38 mg/g of nanoparticles), nanoparticle dose (25, 37, 50, and 75 g/g of Cr(VI)), and initial pH (3, 5, 7, and 9). Results demonstrated the positive impact of acidic pH during Cr(VI) removal by ds-FeS wherein the highest q_m of 31.3 mg/g and initial rate of 6.95 mg/g·min (pseudo-second order kinetics) were observed at pH 3. Conversely, with an increase in pH to neutral and alkaline conditions, a decline in both q_m and initial rates was observed. Measurements of solution pH, total chromium, and particle surface chemistry using X-ray diffraction and Fourier transform infrared spectrometry techniques revealed the crucial roles of reduction, surface precipitation, and complexation processes in Cr(VI) removal by ds-FeS nanoparticles. Overall, this study demonstrates the promising potential of environmentally friendly, date palm seed–derived iron sulfide nanoparticles for Cr(VI) removal.

Keywords Chromium · Date palm · Green synthesis · Heavy metal contaminants · Iron sulfide nanoparticles

F. Habib · A. Shanableh · S. Bhattacharjee (✉) · M. Abdallah
Department of Civil & Environmental Engineering, University of Sharjah, Sharjah, United Arab Emirates
e-mail: sbhattacharjee@sharjah.ac.ae

A. Shanableh
Research Institute of Sciences and Engineering, University of Sharjah, Sharjah, United Arab Emirates

1 Introduction

The presence of hexavalent chromium or Cr(VI), in soil, groundwater, and surface water matrices poses a significant threat to human and environmental health. Cr(VI) typically enters the environment via effluents of industrial processes such as dyeing, metallurgy, and leather tanning and is highly toxic to aquatic species as well as carcinogenic to humans (Guertin, 2004; Mitra et al., 2017; Ukhurebor et al., 2021). Its removal from water systems is therefore critical.

Over the years, a wide range of treatment methods has been evaluated for Cr(VI) removal such as bioremediation, membrane-based separation, adsorption, and chemical reduction and precipitation (Abushawish et al., 2022; Islam et al., 2019; Malaviya & Singh, 2011, 2016; Wang et al., 2019). Reduction and precipitation techniques have seen a wider-scale

implementation, as they allow the economical removal of Cr(VI) by its reduction to trivalent chromium (which has lower toxicity), and subsequent precipitation (Kerur et al., 2021; Ukhurebor et al., 2021). However, a significant challenge with this approach is the requirement for large quantities of dosing chemicals and management of the generated sludge (Malaviya & Singh, 2011). Therefore, more efficient chemical-based approaches are warranted that can separate Cr(VI) from water.

Iron sulfide nanoparticles have shown promise in recent years in contamination abatement applications due to their adsorptive and redox capabilities towards a wide range of pollutants that include organic compounds such as trichloroethylene as well as heavy metals such as mercury and chromium (Gong et al., 2016). Iron sulfide minerals consist of varying compositions of Fe and S (e.g., pyrite FeS_2, greigite Fe_3S_4, and mackinawite FeS) which impart them with contaminant-reducing properties due to the release of Fe^{2+} and reduced sulfur species when in water (Yang et al., 2017). Moreover, in their nanoparticulate form, iron sulfides can also act as effective adsorbents for contaminants due to their large specific surface area and chemically active surface sites (Farooqi et al., 2021). A few studies have investigated the removal of Cr(VI) using different types of iron sulfide nanoparticles (Lyu et al., 2017; Wang et al., 2019; Wu et al., 2017). For instance, Wu et al. (2017) investigated FeS nanoparticles for removal of Cr(VI), and observed a removal capacity of 7.5 mmol Cr(VI) per gram FeS. The authors attributed the removal to both reduction and adsorption processes. Similar mechanisms were involved in the removal of Cr(VI) by Fe_3S_4 nanoparticles as reported by Kong et al. (2022) having a removal capacity of nearly 167 mg g^{-1}. Although not specifically with Cr(VI), Abdul et al. (2019) demonstrated the removal of total chromium by nano-FeS_2 with up to 93% removal of 1 mg/L total chromium at pH 9. Overall iron sulfide nanoparticles have shown a strong potential for Cr(VI) removal and water treatment.

Green synthesis approaches for nanoparticles have generated significant research interest in the past decade due to concerns over the toxicity and environmental footprint of conventional chemical synthesis approaches (Patiño-Ruiz et al., 2021). Plant-derived green synthesis techniques make use of extracts from plant parts, which are abundant in phytochemicals such as polyphenols and flavonoids, to effectively reduce metal precursors into nanoparticles (Bolade et al., 2020). It is crucial to develop and investigate the effectiveness of iron sulfide nanoparticles produced through greener and more eco-friendly synthesis routes, as their utilization in remediation applications continues to rise. Although many methods have been developed for different iron-based nanoparticles (Bolade et al., 2020; Leili et al., 2018; Plachtová et al., 2018), green synthesis approaches for iron sulfide nanoparticles have been scarce. Recently, we proposed a facile approach for preparing iron sulfide nanoparticles by reducing iron sulfate salt by aqueous extracts of date palm (*Phoenix dactylifera*) seeds under mild solution temperature (Bhattacharjee et al., 2021).

The objective of this study was to carry out detailed investigations into the Cr(VI) removal performance of green synthesized iron sulfide nanoparticles and identify the underlying removal mechanisms. This was achieved through a series of batch experiments aimed at determining the Cr(VI) removal capacities and rates of the nanoparticles. Moreover, the effect of reaction conditions such as varying chromium load, varying nanoparticle dose, and the effect of pH was evaluated. We also measured changes in solution pH conditions and particle surface chemistry post the batch experiments to gain insight into the underlying Cr(VI) removal mechanisms. To the best of our knowledge, no studies have been carried out on evaluating the performance of iron sulfide particles produced by green synthesis approach for chromium removal, and this work seeks to bridge the knowledge gap.

2 Materials and Methods

2.1 Chemicals

$FeSO_4.7H_2O$ (99% purity) and K_2CrO_4 (99% purity) were obtained from Sigma Aldrich. ChromaVer3 (Permachem reagent) powder pillows were purchased from Hach. Date seeds were de-pitted from Khalas variety dates (purchased from a local store). Deionized water was used in all experiments.

2.2 Green synthesis of Date Seed Extract–Derived Iron-Sulfide Nanoparticles (ds-FeS)

The sourcing of date seeds, their grinding into powdered form, and the subsequent preparation of their aqueous extract have been described in detail in our previous study (Bhattacharjee et al., 2021). For ds-FeS nanoparticle production, the first 20 mL of $FeSO_4{\cdot}7H_2O$ solution (40 g/L) was mixed with 40 mL of extract. Nanoparticle formation commenced when the mixture was subjected to constant stirring and heated to a temperature of 70 °C. The formed nanoparticles were separated from the solution after 30 min of heating through centrifugation and subsequently lyophilized (Benchtop Pro-Lyophilizer) and stored under anoxic conditions (Korea-Kiyon glove box).

2.3 Characterization Techniques

High-resolution images of the synthesized nanoparticles were obtained using a scanning transmission electron microscopy (STEM) detector fitted to a field emission scanning electron microscope (Thermofisher FEI Apreo C). Size distribution analysis of the nominal particle sizes was carried out by the ImageJ analysis software tool.

X-ray diffraction (XRD) was performed between 10 to 80° using a Bruker D8 instrument with a copper Kα radiation source. Fourier-transform infrared (FTIR) spectroscopy was carried out on dried nanoparticles using Jasco FTIR-6300 instrument. Zeta potential (ζ) of 100 mg/L nanoparticle suspensions was measured using a Litesizer™ 500 particle analyzer in low ionic strength (3 mM NaCl).

2.4 Cr(VI) Removal Experiments

Batch experiments were conducted in uncapped 100 mL Erlenmeyer flasks at room temperature (25 °C), each having a final aqueous volume of 50 mL. Appropriate amounts of K_2CrO_4 were dissolved in water to achieve the final desired Cr(VI) concentrations. The contents of the flask were homogeneously mixed using a magnetic stirrer at 300 rpm. Initial pH adjustments were carried out using HCl or NaOH, before the addition of ds-FeS nanoparticles to the solution.

Maximum Cr(VI) removal capacities were evaluated by adding a fixed dose of ds-FeS nanoparticles to a series of flasks with Cr(VI) concentrations varying from 1.75 to 19 mg/L, at different initial pH levels (pH 3, 7, and 9). Upon nanoparticle addition, the Cr(VI)-nanoparticle suspensions were sonicated briefly and then magnetically stirred for 180 min (the time required to achieve equilibrium). The concentration of ds-FeS nanoparticles was 0.5 g/L.

In kinetic experiments, three sets of conditions were evaluated—effect of chromium load, effect of nanoparticle dose, and effect of varying initial pH values. To evaluate the effect of Cr(VI) load, the ds-FeS nanoparticle concentration was fixed at 0.5 g/L while the Cr(VI) concentration varied between 1.75 and 19 mg/L, whereas to evaluate the effect of nanoparticle dose, the concentration of Cr(VI) was fixed at 13.4 mg/L while the ds-FeS concentration was varied between 0.33 and 1 g/L. Both the effects of varying Cr load and nanoparticle dose were conducted at an initial pH of 7. In the case of varying pH conditions, the Cr(VI) and ds-FeS concentrations were fixed at 13.4 mg/L and 0.5 g/L respectively, while the initial pH conditions were set to 3, 7, and 9. Mixing and handling conditions were similar to what was described earlier. Two replicate systems were set up for all Cr(VI) removal experiments. Cr(VI) removal was assessed by withdrawing 3-mL samples at predetermined time intervals from the flasks and passing the suspension through 0.22-µm syringe filters. The filtered samples were analyzed using a Hach UV–Vis spectrophotometer to determine the residual Cr(VI) concentrations.

2.5 Analytical Techniques

UV–Vis method: Cr (VI) was determined by the 1,5-diphenylcarbohydrazide method using the Hach ChromaVer 3 powder reagent and analyzing absorbance using ultraviolet–visible (UV–Vis) spectrophotometer (model DR 3900; program 90 Chromium, Hex).

Inductively coupled plasma atomic emission spectrometry (ICP-AES): ICP-AES (Thermofisher iCAP 7000 series) was used for the detection of total chromium in solution. Samples were acidified with HCl prior to analysis.

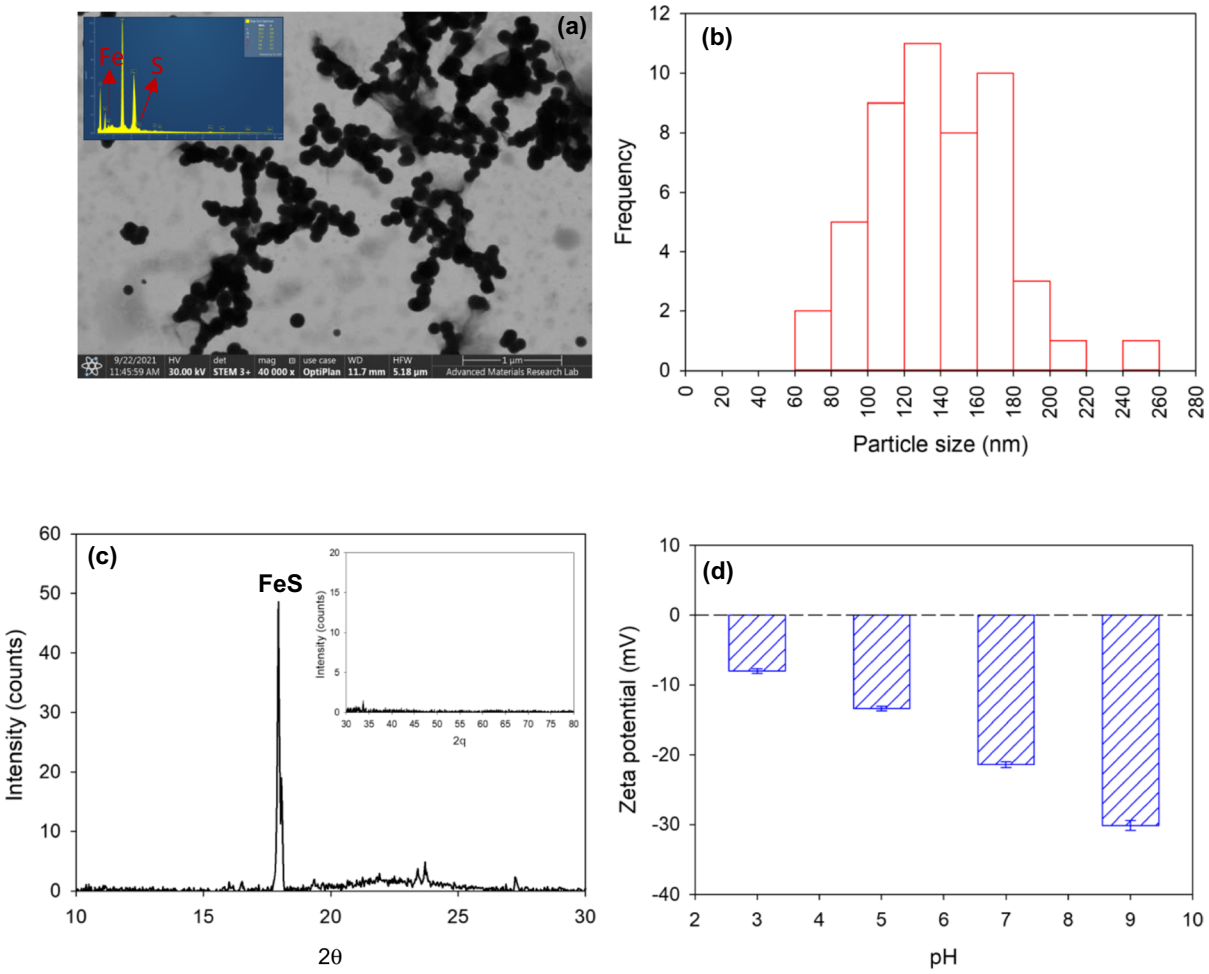

Fig. 1 **a** STEM mode imaging of ds-FeS nanoparticles and **b** corresponding nominal size distribution of ds-FeS nanoparticles; **c** XRD spectra of ds-FeS nanoparticles, inset shows the XRD range between $2\theta = 30$ to 80°; **d** zeta potential of ds-FeS nanoparticles in 3 mM NaCl at different initial pH values

3 Results and Discussion

3.1 Nanoparticle Characterization

Figure 1a presents the high-resolution STEM images of the synthesized nanoparticles. As seen in the figure, the nanoparticles were spherical and arranged in chain-like aggregates. A size distribution of the nominal particle size (Fig. 2b) shows that the majority of the particles were between 100 and 180 nm while a few particles outside this size range were also recorded. The inset in Fig. 1a provides the EDS of the particles wherein we observe peaks for C, O, Fe, S, K, Al, and Au. Al peaks originate from the SEM holding stage whereas Au peaks are observed due to the gold coating procedure employed for the particles for obtaining a clear image. C and O can be attributed to the capping date seed molecules at the nanoparticle surface (Bhattacharjee et al., 2021). Date seeds are rich in minerals such as phosphorus and potassium, which may have leached into the aqueous extracts and likely explain the observation of K peaks in the synthesized nanoparticles (Nehdi et al., 2010). Fe and S peaks in the nanoparticles indicate the formation of iron sulfide due to the reduction of iron sulfate precursor salt as discussed

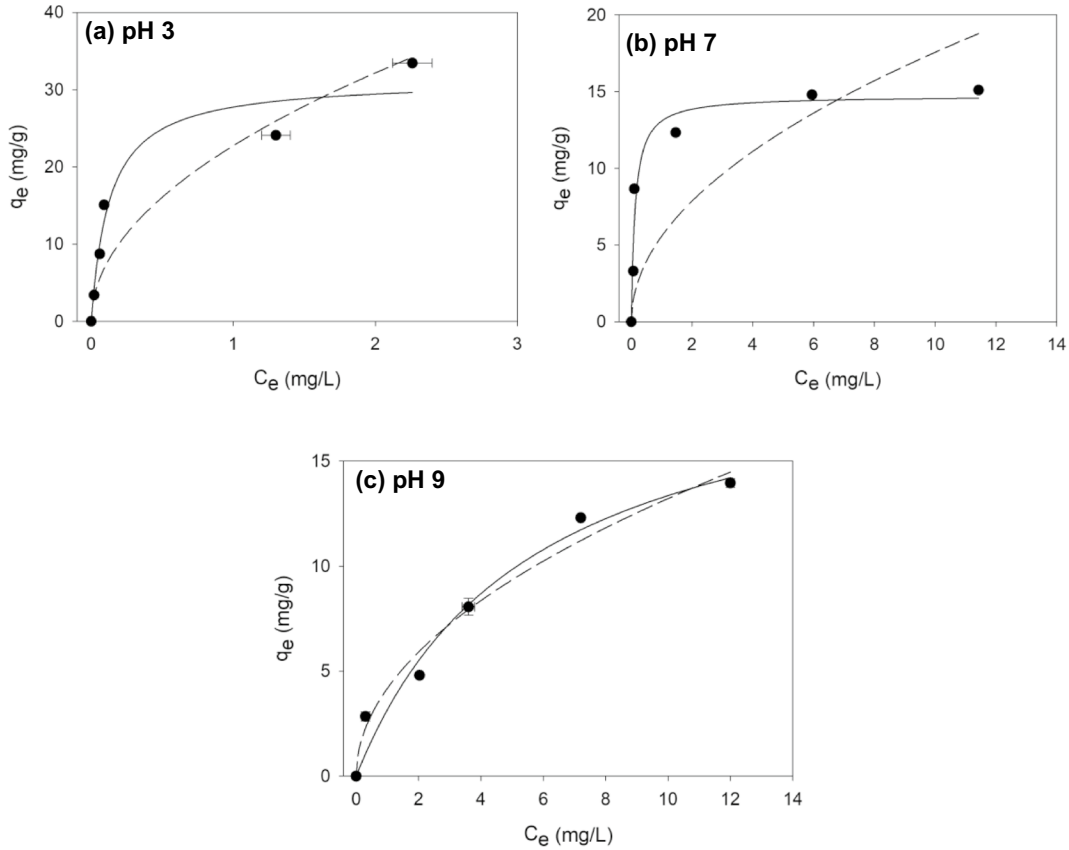

Fig. 2 Cr(VI) removal isotherms at **a** Initial pH 3, **b** initial pH 7, **c** initial pH 9. Solid lines represent Langmuir model fits while dotted lines represent Freundlich model fits. Error bars represent the range of variation between duplicate runs, and when not visible, are smaller than the symbols. Experimental conditions: volume of suspension, 100 mL; nanoparticle concentration, 0.5 g/L; initial Cr (VI) concentrations, varied from 1.75 to 19 mg/L, temperature 25 °C

in the XRD results below and in our previous work (Bhattacharjee et al., 2021).

XRD analysis was performed on the particles and is shown in Fig. 1c. Observed peaks at $2\theta = 17.8°$ and 23.3° are attributable to iron sulfide (mackinawite phase). A low-intensity peak at 27.2° is most likely from the pyrite phase of iron sulfide (Akhtar et al., 2015; Bhattacharjee et al., 2021; Wu et al., 2015).

The zeta potential (ζ) of nanoparticles was also measured to provide insights into the surface charge characteristics of ds-FeS nanoparticles. As seen in Fig. 1d, ds-FeS particles were negatively charged over a wide pH range. The nanoparticles had a $\zeta = -8 \pm 0.3$ mV at pH 3 which decreased to -30 ± 0.7 mV at pH 9. The coating of organic molecules from the date seed extract on the nanoparticle surface likely provides the strong negative charge (Bhattacharjee et al., 2021; Plachtová et al., 2018).

The BET surface area of ds-FeS nanoparticles was 51 m^2/g, as reported in our prior study (Bhattacharjee et al., 2021).

3.2 Chromium Removal Capacity

The equilibrium Cr(VI) removal capacities of the ds-FeS nanoparticles were assessed in batch removal studies at different initial pH conditions (selected to represent acidic, neutral, and basic conditions) and estimated by fitting the data to Langmuir and Freundlich isotherm models shown in Eqs. 1 and 2 respectively.

$$q_e = \frac{q_m k_L C_e}{1 + k_L C_e} \quad (1)$$

$$q_e = k_F C_e^{1/n} \quad (2)$$

where q_e is the Cr(VI) removal capacity attained at equilibrium (mg/g); C_e is the aqueous concentration of Cr(VI) at equilibrium (mg/L); q_m is the maximum Cr(VI) removal capacity (mg/g); k_L represents the Langmuir constant (L/mg)); while k_F and n are Freundlich constants. The model fits of the data are provided in Fig. 2, while Table 1 provides the corresponding fitting parameters.

As seen in Table 1, the Langmuir model adequately described the equilibrium behavior at the initial pH values of 3 and 7, as evidenced by the higher R^2 values compared to the Freundlich model. The Langmuir model also estimated maximum removal capacities close to those obtained experimentally at pH 3 and 7 (Table 1). The adequacy of both Langmuir and Freundlich isotherms for the data at pH 9 based on R^2 values ($R^2 = 0.97$ for both models) may be due to the limited concentration range over which the measurements were carried out at pH 9 (Houng & Lee, 1998). This is also likely why the experimental q_m at pH 9 (14.1 mg/g) is lower than that estimated by the Langmuir model ($q_m = 20.7$ mg/g). For a comparative assessment of the Cr(VI) removal at the different pH levels, we discuss only the Langmuir model parameters below.

From Table 1, we infer that the maximum removal capacity of Cr(VI) was the highest at initial pH 3, with $q_m = 31.3$ mg/g. Changing the initial solution pH to 7 decreased the q_m to 14.7 mg/g. However, at initial pH 9, an increase in q_m was observed with it being 20.7 mg/g. Interestingly, the k_L value at pH 9 was only 0.18 L/mg compared to those at pH 3 (7.8 L/mg) and pH 7 (7.9 L/mg), indicating that the affinity of Cr(VI) for the nanoparticle surface at pH 9 is likely poorer compared to acidic and neutral values (Horsfall Jr et al., 2006).

The Cr(VI) removal capacities obtained in this study were found comparable to those reported in prior literature reports, for nanoparticles prepared via green synthesis approaches (Table 2).

Table 1 Isotherm and kinetic model fitting parameters for Cr(VI) removal by ds-FeS nanoparticles. Units for the terms are q_m (mg/g); k_L (L/mg); q_e (mg/g); k_1 (min^{-1}); k_2 (g/mg· min) respectively. The initial PSO rate (mg/g· min) is represented by $k_2 q_e^2$. "Exp. q_m" represents the experimentally obtained maximum removal capacity (mg/g)

Isotherm model								
Condition	Langmuir			Freundlich				
	q_m	k_L		R^2	k_F	$1/n$	R^2	Exp.q_m
pH 3	31.3	7.8		0.95	22.8	0.5	0.89	33.4
pH 7	14.7	7.9		0.95	5.6	0.5	0.51	13.9
pH 9	20.7	0.2		0.97	4.2	0.5	0.97	14.1
Kinetic model								
Varying parameter	Value	Pseudo-first order			Pseudo-second order			
		q_e	k_1	R^2	q_e	k_2 ($\times 10^{-2}$)	$k_2 q_e^2$	R^2
Cr load mg Cr(VI)/g ds-FeS	3.5	3.2	0.34	0.98	3.3	20.4	2.2	0.99
	9	7.7	0.19	0.89	8.2	3.1	2.1	0.95
	27	11.6	0.15	0.94	12.3	1.7	2.6	0.98
	38	13.0	0.09	0.95	13.8	0.94	1.8	0.98
Nanoparticle dose g ds-FeS/g Cr(VI)	25	9.2	0.15	0.95	10.0	2.3	2.3	0.99
	37	11.6	0.15	0.94	12.3	1.7	2.6	0.98
	50	13.5	0.09	0.92	14.3	0.98	2.0	0.96
	75	11.9	0.17	0.95	13.1	1.9	3.3	0.99
pH	3	24.0	0.18	0.94	25.7	1.1	7.0	0.98
	5	18.3	0.11	0.90	19.8	0.9	3.4	0.96
	7	11.6	0.15	0.94	12.3	1.7	2.6	0.98
	9	10.0	0.15	0.89	10.9	1.8	2.2	0.95

Table 2 Maximum removal capacity of Cr(VI) by different iron-based nanoparticles prepared via green synthesis

Nanoparticles (NPs) used	Maximum Cr(VI) removal capacity (mg/g)	Reference
Zerovalent iron NPs prepared using *E. globules* leaf extract	5.5	Madhavi et al. (2013)
Fe -NPs prepared using eucalyptus leaf extract	20.5	Jin et al. (2018)
Zerovalent iron NPs prepared using Citrus limetta peels	33.3	Dalal and Reddy (2019)
Fe -NPs prepared from pear peel extract	46.6	Rong et al. (2020)
Iron sulfide NPs prepared using date seed extract	31.3	This study

3.3 Chromium Removal Mechanism

A number of studies have suggested the role of electrostatic adsorption between nanoparticle surfaces and Cr(VI) species in solution, on the overall Cr(VI) removal process (Ukhurebor et al., 2021). Within the range of pH levels investigated in this study, Cr(VI) exists predominantly as $HCrO_4^-$ anion at pH 3, as both CrO_4^{2-} and $HCrO_4^-$ at pH 7, and as CrO_4^{2-} at pH 9 (Bandara et al., 2020; Zhang et al., 2019). However, as observed in Fig. 1d, ds-FeS particles show an increasingly negative zeta potential through the pH range of 3 to 9. Nanoparticles displayed $\zeta = -8 \pm 0.3$ mV at pH 3, -21 ± 0.4 mV at pH 7, and -30 ± 0.7 mV at pH 9. The anionic charges of both the ds-FeS particles and the chromate anions suggest that electrostatic adsorption of Cr(VI) may not be the dominant factor contributing to its removal. Therefore, we carried out comparative measurements of solution properties and nanoparticle surface chemistry, before and after batch experiments, to probe the underlying Cr(VI) removal mechanisms. This was done at the initial Cr(VI) concentration of 13.4 mg/L, which was an intermediate point among the range of concentrations tested for the isotherm experiment.

Figure 3a provides the solution phase measurements of Cr(VI) and Total Cr post the batch experiments, at different initial pH conditions. The control system represents the measurements of the solution phase chromium without nanoparticle exposure and demonstrates that all the chromium existed in the hexavalent state as indicated by the similar values of Total Cr and Cr (VI). After exposing the ds-FeS nanoparticles to Cr (VI) at initial pH 3, the Cr(VI) in solution decreased to 1.5 mg/L whereas the amount of Total Cr in solution was higher at 5 mg/L. The difference of 3.5 mg/L (total Cr − Cr(VI)) can be attributed to the presence of dissolved Cr (III) in the solution. The net amount of chromium removed from the solution compared to the control system is likely due to the formation of surface Cr (III) oxide precipitates as discussed below.

We also observe an increase in solution pH (Fig. 3b) from an initial pH of 3 to a final pH of 4 after exposure of ds-FeS to Cr(VI). Thus under acidic conditions, it is likely that the dissolution of FeS to Fe^{2+} and HS^- ions took place followed by the reduction of Cr (VI) to Cr (III) and subsequent precipitation of some Cr-oxides, as shown in the equations below (Lyu et al., 2017; Wang et al., 2019):

$$FeS + H^+ \rightarrow Fe^{2+} + HS^- \quad (1)$$

$$3Fe^{2+} + HCrO_4^- + 7H^+ \rightarrow 3Fe^{3+} + Cr^{3+} + 4H_2O \quad (2)$$

$$HS^- + 2HCrO_4^- + 7H^+ \rightarrow SO_3^{2-} + 2Cr^{3+} + 5H_2O \quad (3)$$

$$8HS^- + 3HCrO_4^- + 29H^+ \rightarrow 3SO_4^{2-} + 8Cr^{3+} + 20H_2O \quad (4)$$

$$xCr^{3+} + (1-x)Fe^{3+} + 3H_2O \rightarrow (Cr_xFe_{1-x})(OH_{3(S)}) + 3H^+ \quad (5)$$

In Fig. 3a, we observe that at initial pH 7 and pH 9, all of the chromium measured in solution post-exposure to nanoparticles existed in the hexavalent form (as indicated by the similar total Cr and Cr(VI) values). Additionally, we observe that in Fig. 3b, the pH of the solutions after reaction with ds-FeS decreased from initial pH values of 7 and 9 to final pH values of 5 and 5.5 respectively.

This suggests that the removal mechanism under more neutral to alkaline conditions may likely involve the reduction of Cr(VI) (present as CrO_4^{2-}) to Cr (III)

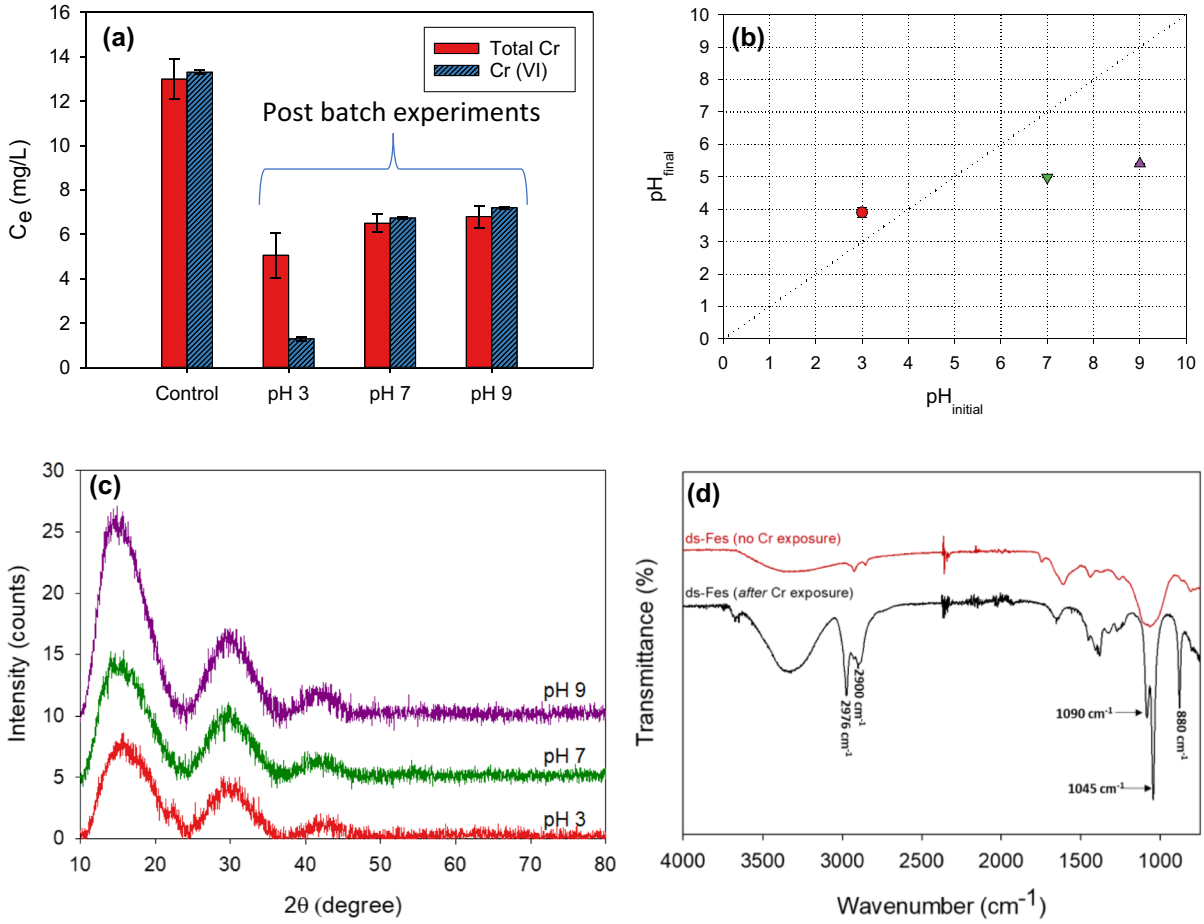

Fig. 3 **a** Solution phase measurements of Total Cr and Cr(VI) before and after batch experiments, error bars represent the range of variation between duplicate runs, **b** pH measurements of solution before and after batch experiments, **c** XRD of ds-FeS after batch experiments, **d** FTIR spectra of ds-FeS nanoparticles before and after batch experiments, at pH 7

oxides followed by surface precipitation of $Fe(OH)_3$ and $Cr(OH)_3$, as shown in Eq. (6) below (Zheng et al., 2020). The absence of Cr(III) in solution suggests that minimal dissolution of Cr-oxides may have occurred.

$$3Fe^{+2} + CrO_4^{2-} + 8H_2O \rightarrow 3Fe(OH)_3 + Cr(OH)_3 + 4H^+ \quad (6)$$

The deposition of Cr-oxides on the nanoparticle surface likely results in monolayer coverage as indicated by the appropriateness of the Langmuir isotherm model in fitting the data (Table 1).

Further investigation of the nanoparticles was carried out using XRD post-batch experiments and is shown in Fig. 3c. The diffraction pattern of the particles retrieved from the three pH solutions (initial pH 3, 7, and 9) looked similar, albeit certain peak intensities were different. Compared to pristine ds-FeS nanoparticles (Fig. 1c), broad peaks centered around $2\theta = 14.8°$, 29.8°, and 42.5° were observed for Cr(VI) exposed nanoparticles in Fig. 3c. The broadened peaks indicate the less crystallized nature of the reaction products. The peak at 14.8° may be attributed to Cr–O products while the peak at 29.8° likely indicates $FeCr_2O_4$ (Zhou et al., 2022). ds-FeS particles retrieved from solutions in more alkaline pH appeared to have a higher intensity of peaks at 14.8° and 29.8° which could be due to a higher coprecipitation of Cr-oxide products on the particle surface. The diffraction peak at 42.5° is likely due to the formation of iron oxides such as magnetite and lepidocrocite γ-FeO(OH) (Liu et al., 2017).

Prior studies have suggested the involvement of nanoparticle capping molecules in the chemisorption of Cr(VI) through complexation (Mehmood et al., 2022). We therefore also carried out a comparative analysis of the surface functional groups of the ds-FeS particles before and after Cr(VI) batch experiments.

Figure 3d provides the FTIR spectra for ds-FeS nanoparticles before and after exposure to Cr(VI) in batch experiments investigated at a selected initial pH of 7. The FTIR spectra for pristine ds-FeS nanoparticles (not exposed to Cr(VI)) have been presented and discussed in our prior study as well (Bhattacharjee et al., 2021). The spectral analysis revealed the presence of several surface functional groups on pristine ds-FeS nanoparticles, which are from the date seed extract molecules involved in the synthesis and capping process (Bhattacharjee et al., 2021). The peaks at 2855 cm^{-1} and 2925 cm^{-1} can be attributed to the asymmetric and symmetric C-H stretches from alkyl groups, respectively. After exposure to Cr(VI), the aforementioned peaks showed shifts to 2900 and 2976 cm^{-1} respectively. The peaks in the region 800–1500 cm^{-1} in pristine ds-FeS particles are attributable to the fingerprint region of the capping date seed extract organic molecules. The most significant differences in the ds-FeS particles after exposure to Cr(VI) occurred in this region. The broad peak of ds-FeS (before Cr exposure) at 1061 cm^{-1} was replaced by two sharp peaks at 1045 cm^{-1} and 1090 cm^{-1} after exposure to Cr(VI), which can be attributed to C–O–C and C-O stretching respectively (Chen et al., 2016). An additional peak also appeared at 880 cm^{-1} for ds-FeS nanoparticles after exposure to Cr(VI). Overall, the comparison of the FTIR spectra for ds-FeS nanoparticles before and after exposure to Cr(VI) indicates that functional groups of the capping molecules may also be involved in the overall removal process through complexation of Cr(VI) or the transformed Cr(III) ions.

3.4 Chromium Removal Kinetics

The kinetics of Cr(VI) removal are shown in Fig. 4a–c, under conditions of varying initial Cr(VI) load (Fig. 4a), varying nanoparticle dose (Fig. 4b), and different initial pH (Fig. 4c). Under all scenarios investigated, removal of Cr(VI) was rapid achieving 80–90% of the equilibrium removal capacity within 30 min. The pseudo-first-order (PFO) and pseudo-second-order (PSO) kinetic models were used to fit the kinetic removal data, as shown in equations below.

$$q_t = q_e(1 - e^{-k_1 t}) \tag{7}$$

$$q_t = \frac{k_2 q_e^2 t}{1 + k_2 q_e t} \tag{8}$$

where q_t (mg/g) is the Cr(VI) removed by ds-FeS at time t while q_e (mg/g) is that removed at equilibrium. The PFO rate constant and PSO rate constant is represented by k_1 (min^{-1}) and k_2 (g/mg· min) respectively. The initial PSO rate (mg/g· min) is represented by $k_2 q_e^2$.

The kinetic parameters obtained under the various conditions are presented in Table 1. As shown in the table, the correlation coefficients were higher for the PSO model suggesting its appropriateness in representing the kinetic data. The goodness of fit to the PSO model also indicates that the removal mechanism likely occurs via chemisorption processes, which is in agreement with the removal mechanisms discussed earlier (Section 3.3). To obtain an insight into the effects of the varying conditions on the rate of Cr(VI) removal, the PSO initial rates are plotted in Fig. 4d–f.

In Fig. 4d, we observe that varying the initial Cr(VI) load (at fixed nanoparticle concentration and pH) did not impact the initial rates drastically within the concentration range investigated. For instance, a 10 times increase in the Cr(VI) load from 3.5 to 38 mg Cr/g nanoparticles displayed an initial rate averaging around 2.5 mg/g· min. The lack of change in the initial rate likely indicates a sufficient amount of reactive species for facilitating Cr(VI) removal.

In Fig. 4e, the change in initial rates is shown with changing nanoparticle load. We observe that up to 50 g nanoparticle/g of Cr, the initial rates show minimal variation and also average around 2.5 mg/g· min. At a higher dose of 75 g nanoparticles/g Cr, we see a slight improvement in the rate to 3.26 mg/g· min. The improvement may be due to an increase in the amount of nanoparticle surface sites and or dissolved reactive Fe species which facilitate faster Cr(VI) transformation and thus a higher reaction rate.

However, the most significant impact on the reaction rates was that of varying the initial solution pH as observed in Fig. 4e. The highest rates were observed in acidic pH. For instance, at pH 3, we observe the highest initial rate of 6.95 mg/g· min which decreased to 3.36 mg/g· min at pH 5. The initial rates progressively decreased and appeared to plateau in neutral to

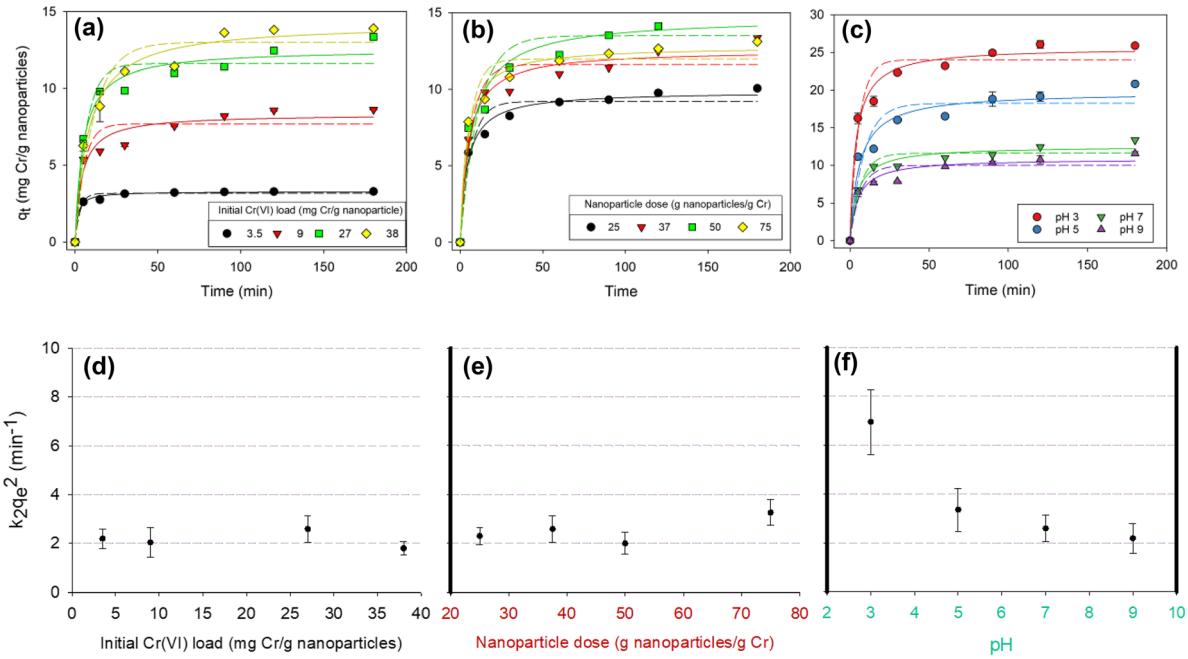

Fig. 4 Top panel represents the kinetics of Cr(VI) removal and bottom panel represents PSO initial rates for conditions of—varying initial Cr(VI) load (**a** and **d**), varying nanoparticle dose (**b** and **e**), and varying initial pH (**c** and **f**); dotted lines represent pseudo second order model fits while solid lines are pseudo first order model fits in parts **a**–**c**. Error bars represent the range of variation between duplicate runs and, when not visible, are smaller than the symbols

alkaline conditions with them being 2.59 mg/g· min at pH 7 and 2.2 mg/g· min at pH 9. As discussed earlier, the acidic conditions are favorable for the formation of more dissolved iron and sulfide species which can accelerate the reduction of Cr(VI) to Cr(III).

4 Conclusion

This study effectively employed novel iron sulfide nanoparticles derived from date seed extracts to remove Cr(VI) from aqueous solutions. The optimal conditions for Cr(VI) removal were found to be under acidic conditions (initial pH 3), resulting in a maximum removal capacity of 31.3 mg/g and a rapid removal rate of 6.95 mg/g·min, as determined by Langmuir isotherm and pseudo-second-order kinetics, respectively. Conversely, at pH 9, the removal capacity dropped to 20.7 mg/g, and the removal rate decreased to 2.2 mg/g·min. The underlying mechanism of Cr(VI) removal involved the reduction of Cr(VI) to Cr(III) by dissolved Fe^{2+}/HS^{-} species, followed by the surface precipitation of Cr-oxides. These processes were more favorable in acidic conditions, emphasizing the importance of pH in the removal process. Interestingly, varying the concentrations of Cr(VI) or ds-FeS nanoparticles had minimal impact on the initial reaction rates. Additionally, it was observed that organic capping molecules on the surface of ds-FeS nanoparticles played a significant role in the removal of Cr(VI), likely through complexation.

In conclusion, this study demonstrated the effectiveness of iron sulfide nanoparticles produced via the green synthesis approach in transforming Cr(VI) into less toxic forms. To gain a more comprehensive understanding of the performance of these nanoparticles for Cr(VI) removal, future research should explore the effects of competing ions, dissolved organic matter, and complex water matrices.

Acknowledgements We thank the Center of Advanced Materials Research at UoS for the assistance with the characterization of nanoparticles.

Funding This work was funded by the University of Sharjah (UoS) grant number UoS-130508, PI: A. Shanableh.

Data Availability The datasets are available from the corresponding author upon request.

Declarations

Competing Interests The authors declare no competing interests.

References

Abdul, N. A., Abdul-Talib, S., & Amir, A. (2019). Nano-pyrite as a reductant to remove chromium in groundwater. *KSCE Journal of Civil Engineering, 23*, 992–999.

Abushawish, A., Almanassra, I. W., Backer, S. N., Jaber, L., Khalil, A. K., Abdelkareem, M. A., Sayed, E. T., Alawadhi, H., Shanableh, A., & Atieh, M. A. (2022). High-efficiency removal of hexavalent chromium from contaminated water using nitrogen-doped activated carbon: Kinetics and isotherm study. *Materials Chemistry and Physics, 291*, 126758.

Akhtar, M. S., Alenad, A., & Malik, M. A. (2015). Synthesis of mackinawite FeS thin films from acidic chemical baths. *Materials Science in Semiconductor Processing, 32*, 1–5.

Bandara, P., Peña-Bahamonde, J., & Rodrigues, D. (2020). Redox mechanisms of conversion of Cr (VI) to Cr (III) by graphene oxide-polymer composite. *Scientific Reports, 10*, 1–8.

Bhattacharjee, S., Habib, F., Darwish, N., & Shanableh, A. (2021). Iron sulfide nanoparticles prepared using date seed extract: Green synthesis, characterization and potential application for removal of ciprofloxacin and chromium. *Powder Technology, 380*, 219–228.

Bolade, O. P., Williams, A. B., & Benson, N. U. (2020). 'Green synthesis of iron-based nanomaterials for environmental remediation: A review', Environmental Nanotechnology. *Monitoring & Management, 13*, 100279.

Chen, W., Chen, S., Morsi, Y., El-Hamshary, H., El-Newhy, M., Fan, C., & Mo, X. (2016). Superabsorbent 3D scaffold based on electrospun nanofibers for cartilage tissue engineering. *ACS Applied Materials & Interfaces, 8*, 24415–24425.

Dalal, U., & Reddy, S. N. (2019). A novel nano zero-valent iron biomaterial for chromium (Cr6+ to Cr3+) reduction. *Environmental Science and Pollution Research, 26*, 10631–10640.

Farooqi, Z. H., Akram, M. W., Begum, R., Wu, W., & Irfan, A. (2021). Inorganic nanoparticles for reduction of hexavalent chromium: Physicochemical aspects. *Journal of Hazardous Materials, 402*, 123535.

Gong, Y., Tang, J., & Zhao, D. (2016). Application of iron sulfide particles for groundwater and soil remediation: A review. *Water Research, 89*, 309–320.

Guertin, J. (2004). *'Toxicity and health effects of chromium (all oxidation states)* (pp. 215–234). Chromium (VI) handbook.

Horsfall, M., Jr., Ogban, F., & Akporhonor, E. E. (2006). Sorption of chromium (VI) from aqueous solution by cassava (Manihot sculenta Cranz.) waste biomass. *Chemistry & Biodiversity, 3*, 161–174.

Houng, K.-H., & Lee, D.-Y. (1998). 'Comparisons of linear and nonlinear Langmuir and Freundlich curve-fit in the study of Cu, Cd and Pb adsorption on Taiwan soils. *Soil Science, 163*, 115–121.

Islam, M. A., Angove, M. J., & Morton, D. W. (2019). 'Recent innovative research on chromium (VI) adsorption mechanism', Environmental Nanotechnology. *Monitoring & Management, 12*, 100267.

Jin, X., Liu, Y., Tan, J., Owens, G., & Chen, Z. (2018). Removal of Cr (VI) from aqueous solutions via reduction and absorption by green synthesized iron nanoparticles. *Journal of Cleaner Production, 176*, 929–936.

Kerur, S., Bandekar, S., Hanagadakar, M. S., Nandi, S. S., Ratnamala, G., & Hegde, P. G. (2021). Removal of hexavalent Chromium-Industry treated water and Wastewater: A review. *Materials Today: Proceedings, 42*, 1112–1121.

Kong, L., Yan, R., Liu, M., Xu, J., Hagio, T., Ichino, R., Li, L., & Cao, X. (2022). Simultaneous reduction and sequestration of hexavalent chromium by magnetic β-Cyclodextrin stabilized Fe3S4. *Journal of Hazardous Materials, 431*, 128592.

Leili, M., Fazlzadeh, M., & Bhatnagar, A. (2018). Green synthesis of nano-zero-valent iron from Nettle and Thyme leaf extracts and their application for the removal of cephalexin antibiotic from aqueous solutions. *Environmental Technology, 39*, 1158–1172.

Liu, A., Liu, J., Han, J., & Zhang, W.-X. (2017). 'Evolution of nanoscale zero-valent iron (nZVI) in water: Microscopic and spectroscopic evidence on the formation of nano-and micro-structured iron oxides. *Journal of hazardous materials, 322*, 129–135.

Lyu, H., Tang, J., Huang, Y., Gai, L., Zeng, E. Y., Liber, K., & Gong, Y. (2017). Removal of hexavalent chromium from aqueous solutions by a novel biochar supported nanoscale iron sulfide composite. *Chemical Engineering Journal, 322*, 516–524.

Madhavi, V., Prasad, T., Reddy, A. V. B., Reddy, B. R., & Madhavi, G. (2013). Application of phytogenic zerovalent iron nanoparticles in the adsorption of hexavalent chromium. *Spectrochimica Acta Part a: Molecular and Biomolecular Spectroscopy, 116*, 17–25.

Malaviya, P., & Singh, A. (2011). Physicochemical technologies for remediation of chromium-containing waters and wastewaters. *Critical Reviews in Environmental Science and Technology, 41*, 1111–1172.

Malaviya, P., & Singh, A. (2016). Bioremediation of chromium solutions and chromium containing wastewaters. *Critical Reviews in Microbiology, 42*, 607–633.

Mehmood, S., Mahmood, M., Núñez-Delgado, A., Alatalo, J. M., Elrys, A. S., Rizwan, M., Weng, J., Li, W., & Ahmed, W. (2022). A green method for removing chromium (VI) from aqueous systems using novel silicon nanoparticles: Adsorption and interaction mechanisms. *Environmental Research, 213*, 113614.

Mitra, S., Sarkar, A., & Sen, S. (2017). Removal of chromium from industrial effluents using nanotechnology: A review. *Nanotechnology for Environmental Engineering, 2*, 1–14.

Nehdi, I., Omri, S., Khalil, M., & Al-Resayes, S. (2010). Characteristics and chemical composition of date palm (Phoenix canariensis) seeds and seed oil. *Industrial Crops and Products, 32*, 360–365.

Patiño-Ruiz, D. A., Meramo-Hurtado, S. I., González-Delgado, Á. D., & Herrera, A. (2021). Environmental sustainability

evaluation of iron oxide nanoparticles synthesized via green synthesis and the coprecipitation method: A comparative life cycle assessment study. *ACS Omega, 6*, 12410–12423.

Plachtová, P., Medrikova, Z., Zboril, R., Tucek, J., Varma, R. S., & Maršálek, B. (2018). Iron and iron oxide nanoparticles synthesized with green tea extract: Differences in ecotoxicological profile and ability to degrade malachite green. *ACS Sustainable Chemistry & Engineering, 6*, 8679–8687.

Rong, K., Wang, J., Zhang, Z., & Zhang, J. (2020). Green synthesis of iron nanoparticles using Korla fragrant pear peel extracts for the removal of aqueous Cr (VI). *Ecological Engineering, 149*, 105793.

Ukhurebor, K. E., Aigbe, U. O., Onyancha, R. B., Nwankwo, W., Osibote, O. A., Paumo, H. K., Ama, O. M., Adetunji, C. O., & Siloko, I. U. (2021). Effect of hexavalent chromium on the environment and removal techniques: A review. *Journal of Environmental Management, 280*, 111809.

Wang, T., Liu, Y., Wang, J., Wang, X., Liu, B., & Wang, Y. (2019). In-situ remediation of hexavalent chromium contaminated groundwater and saturated soil using stabilized iron sulfide nanoparticles. *Journal of Environmental Management, 231*, 679–686.

Wu, J., Liang, Y., Bai, P., Zheng, S., & Chen, L. (2015). Microwave-assisted synthesis of pyrite FeS 2 microspheres with strong absorption performance. *RSC Advances, 5*, 65575–65582.

Wu, J., Wang, X.-B., & Zeng, R. J. (2017). Reactivity enhancement of iron sulfide nanoparticles stabilized by sodium alginate: Taking Cr (VI) removal as an example. *Journal of Hazardous Materials, 333*, 275–284.

Yang, Y., Chen, T., Sumona, M., Gupta, B. S., Sun, Y., Hu, Z., & Zhan, X. (2017). Utilization of iron sulfides for wastewater treatment: A critical review. *Reviews in Environmental Science and Bio/technology, 16*, 289–308.

Zhang, H., Peng, L., Chen, A., Shang, C., Lei, M., He, K., Luo, S., Shao, J., & Zeng, Q. (2019). Chitosan-stabilized FeS magnetic composites for chromium removal: Characterization, performance, mechanism, and stability. *Carbohydrate Polymers, 214*, 276–285.

Zheng, Y., Liu, S., Dai, C., Duan, Y., Makhinov, A. N., Hon, L. K., & Araruna Júnior, J. T. (2020). Study on the influence mechanism of underground mineral element Fe (II) on Cr (VI) transformation under subsurface and groundwater interaction zones. *Environmental Sciences Europe, 32*, 1–14.

Zhou, C., Han, C., Min, X., & Yang, T. (2022). Effect of different sulfur precursors on efficient chromium (VI) removal by ZSM-5 zeolite supporting sulfide nano zero-valent iron. *Chemical Engineering Journal, 427*, 131515.

Publisher's Note Springer Nature remains neutral with regard to jurisdictional claims in published maps and institutional affiliations.

Springer Nature or its licensor (e.g. a society or other partner) holds exclusive rights to this article under a publishing agreement with the author(s) or other rightsholder(s); author self-archiving of the accepted manuscript version of this article is solely governed by the terms of such publishing agreement and applicable law.